Miner Deposita (2014) 49:809–819
DOI 10.1007/s00126-014-0536-1

LETTER

Cooling and exhumation of the mid-Jurassic porphyry copper systems in Dexing City, SE China: insights from geo- and thermochronology

Xuan Liu · Hong-rui Fan · Noreen J. Evans · Geoffrey E. Batt · Brent I. A. McInnes · Kui-feng Yang · Ke-zhang Qin

Received: 10 April 2014 / Accepted: 23 June 2014 / Published online: 14 August 2014

Abstract The Dexing porphyry copper and Yinshan polymetallic deposits in Dexing City, southeastern China are both giant porphyry ore systems. Located 15 km apart, they formed synchronously and share a similar magma source and metallogenic evolution, but their metal endowment, dominant rock types, and alteration assemblages differ significantly. In this contribution, we investigate the cause of these distinctions through new molybdenite Re–Os ages and zircon and apatite (U–Th)/He thermochronology data. Dexing has a molybdenite Re–Os age of ~170.3 Ma, zircon (U–Th)/He (ZHe) ages of 110 to 120 Ma and apatite (U–Th)/He (AHe) ages of 7 to 9 Ma. In contrast, Yinshan has older ZHe ages of 128 to 140 Ma and an AHe age of ~30 Ma. Viewed in combination with previously published data, we conclude that the apparently slow cooling experienced by these bodies is primarily a reflection of their experiencing multiple episodes of thermal disturbance. We tentatively infer that both deposits were exposed in the Late Miocene or more recent time, with the Dexing deposit more deeply exhumed than Yinshan. Our study has exploration implications for deeper porphyry-style ores at Yinshan and for porphyry deposits in non-arc (intraplate) settings in general.

Editorial handling: T. Bissig

X. Liu · H.-r. Fan (✉) · K.-f. Yang · K.-z. Qin
Key Laboratory of Mineral Resources, Institute of Geology and Geophysics, Chinese Academy of Sciences, Beijing 100029, China
e-mail: fanhr@mail.iggcas.ac.cn

N. J. Evans · B. I. A. McInnes
John de Laeter Centre for Isotope Research, Department of Applied Geology, Curtin University, Perth 6845, Australia

G. E. Batt
Center for Exploration Targeting, School of Earth and Environment, University of Western Australia, Crawley 6009, Australia

Keywords Dexing porphyry Cu deposit · Yinshan polymetallic deposit · (U–Th)/He · Thermochronology · Cooling · Exhumation

Introduction

Porphyry deposits are normally formed by late magmatic and hydrothermal processes several kilometers (typically 1–5 km) deep in the upper crust (Seedorff et al. 2005), and their presence at economically accessible levels demonstrates an additional history of tectonic and/or erosional exhumation (Kesler and Wilkinson 2006). Examining the record of post-mineralization cooling and exhumation for a prospective region thus represents a potentially valuable contribution to prediction of the presence and character of porphyry-style mineral endowment.

The closure temperature (T_c) of helium is approximately ~200 °C for zircon and ~75 °C for apatite, respectively (Wolf et al. 1996; Reiners and Farley 1999; Farley 2000; Farley and Stöckli 2002; Reiners 2005). It follows that a zircon (U–Th)/He age for porphyry mineralization probably records the timing of the latest hydrothermal event to have affected the system, whereas an apatite (U–Th)/He age is more likely related to thermal collapse and/or unroofing. A combination of these two ages can thus provide valuable information regarding the post-mineralization uplift and exhumation history of ore deposits, with significant implications for ore preservation (McInnes et al. 2005a). More importantly, if these two constraints are combined with other chronometers such as zircon U/Pb (T_c>900 °C; Cherniak and Watson 2000) and Re–Os (T_c=440–500 °C; Suzuki et al. 1996; Selby and Creaser 2001), a thermal history spanning over 800 °C can be elucidated.

The Dexing and Yinshan deposits are nearly identical in terms of magma genesis (Wang et al. 2012a; Liu et al. 2013) and formation age (Li et al. 2007; Zhou et al. 2011), and were emplaced into the same country rocks. However, their metal endowment, rock character, and alteration assemblages differ significantly. Dexing is dominated by porphyry Cu–Au–Mo ores hosted by porphyritic rocks whereas Yinshan comprises epithermal Pb–Zn–Ag veins and coeval volcanic rocks. We here re-evaluate the cooling history of the two ore deposits in order to determine the degree to which differential exhumation may be a factor in their contrasting preservation and to establish preliminary thermal history relationships between the two.

Regional geology

Dexing City in Jiangxi Province is one of the most important Cu–Pb–Zn and Au mining districts in SE China (Hua et al. 2000). It is located in the eastern segment of a Neoproterozoic orogen (commonly referred to as the "Jiangnan Orogen"; Fig. 1a; Wang et al. 2012b) formed during amalgamation of the Yangtze and Cathaysia terranes to form the South China Block. The basement rocks of this area are separated by the Northeast Jiangxi Fault Belt and consist of two rock units: the early Neoproterozoic greenschist facies volcano-sedimentary Shuangqiaoshan Group (Wang et al. 2008) and a tectonically complex terrane of disrupted turbidities and early Neoproterozoic arc-related rocks assigned to the Qigong Group (Li et al. 2009). Locally, the basement rocks are unconformably overlain by Cambrian to Cenozoic strata.

The oldest structures in the Dexing and surrounding areas are ENE-trending folds developed within the Shuangqiaoshan Group and associated E-trending faults (Fig. 1b). This fabric was overprinted during the Paleozoic and Mesozoic by NE-trending faults and subordinate fold structures, with the region then disrupted by Jurassic and Cretaceous extension and the development of several significant fault-bounded basins (JGB 1980). These late graben include such significant depocenters as the Leping–Dexing basin, which accommodates basal Upper Jurassic volcanic tuff and breccias (~270 m in thickness) overlain by greater than 1,800 m of Lower Cretaceous lacustrine facies sediments (Fig. 1c). The region was later affected by a further phase of NNE-trending faulting and by a final phase of extension producing a suite of NW-trending normal faults cross-cutting all earlier structures.

Deposit geology

General geology of the Dexing deposit

The Dexing porphyry copper deposit (Fig. 1e; with a resource estimate of 1,700 Mt of ore at 0.5 % Cu, 0.02 % Mo, and 0.011 g/t Au; Huang et al. 2001) is hosted by three granodiorite porphyry stocks (Zhushahong, Tongchang, and Fujiawu) emplaced into the phyllite and slate of the Shuangqiaoshan Group. Early hydrothermal alteration resulted in an inner zone of potassic assemblages and an outer zone of propylitic rocks, which is partially overprinted by later intense phyllic alteration along the contact zones between the porphyries and their wallrocks. Mineralization is dominated by sulfide veinlets, stockworks, and disseminated sulfides, with primary ore minerals consisting of pyrite, chalcopyrite, and molybdenite, together with minor bornite, tennantite, and bismuth-bearing copper sulfide. Ore bodies (Fig. 1e) are primarily contained in the phyllic alteration zone, the top of which has been exhumed by tectonic unroofing (Hou et al. 2013).

Previous chronological work on the Dexing deposit

Magmatic rocks at Dexing consist of granodiorite porphyries, minor granitic aplite, and quartz diorite dykes. Zircon U–Pb dating by laser ablation inductively coupled mass spectrometry (LA-ICPMS; Wang et al. 2006; Zhou et al. 2011; Liu et al. 2012) indicates an intrusion age for the granodiorite porphyries of 170–173 Ma. Initial mineralization is contemporaneous with this emplacement episode, with molybdenite from molybdenite–pyrite–quartz veins yielding a well-defined Re–Os age of ~170 Ma (Zhou et al. 2011). Cross-cutting relationships demonstrate that the granitic aplite formed after emplacement of the porphyries but before potassic alteration (Zhu et al. 1983). Zhou et al. (2012a) reported a SHRIMP zircon U–Pb age of ~153.5 Ma for a quartz diorite dyke, with Zhu et al. (1983) obtaining K–Ar ages of 152–157 Ma from quartz–K-feldspar veins and a K–Ar age of ~112 Ma for hydrothermal illite of the altered granodiorite porphyry. These K–Ar ages are not considered good estimates of the timing of mineralization, but they are potential thermo-chronometers, recording the time at which their host minerals passed through the relevant closure temperatures of ~230 °C for K-feldspar (Suzuki et al. 1996) and ~150 °C for illite (Hamilton et al. 1989). Zhou et al. (2012b) reported SHRIMP U–Pb ages of 101–107 Ma for hydrothermal zircon from a structurally late pyrite–chalcopyrite–quartz vein, demonstrating the occurrence of a distinct later episode of hydrothermal activity at Dexing.

General geology of the Yinshan deposit

The Yinshan deposit (Fig. 1d) hosts estimated ore resources of 83 Mt at 0.5 % Cu, 0.8 g/t Au, 1.3 % Pb, 1.0 % Zn, and 33.3 g/t Ag (Wang et al. 2013). Exposed lithologies include subvolcanic rocks (dacite porphyries, quartz porphyries, quartz diorite porphyries, and andesite porphyries), voluminous volcanic and volcaniclastic materials, breccias, and Shuangqiaoshan metamorphic rocks (primarily phyllite). Hydrothermal alteration is dominated

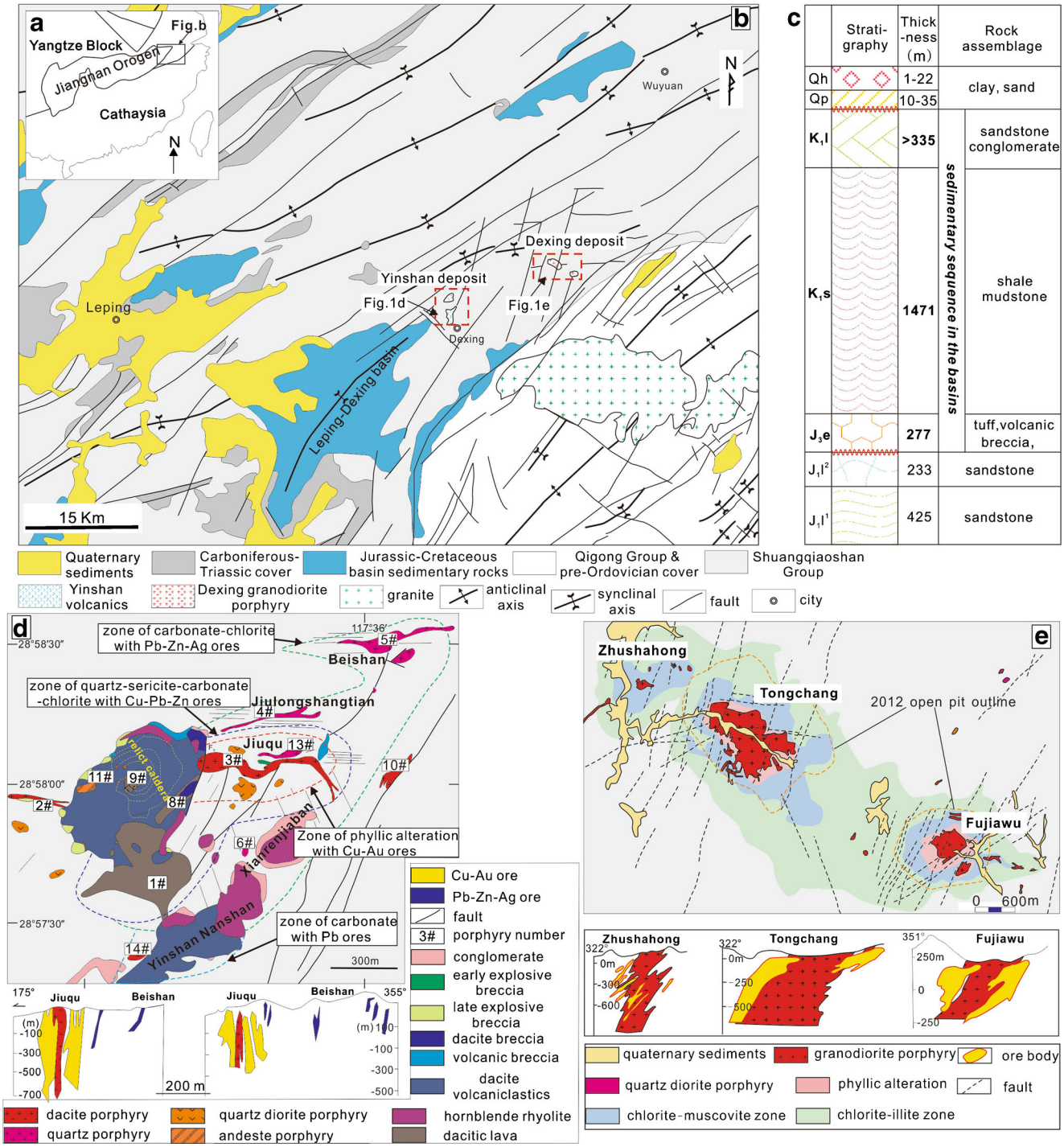

Fig. 1 Geological map of the Dexing area, Dexing deposit and Yinshan deposit (**a** is modified after Liu et al. (2012); **b** is modified after JGB Jiangxi Geological Bureau (1980); **c** is a stratigraphic column of the Dexing region and its surrounding area, shortened since the Jurassic; **d** is geological map of the Yinshan deposit (modified after JGEB 1996); and **e** is geological map of the Dexing deposit (modified after Zhu et al. 1983))

by phyllic and propylitic assemblages which show systematic zonation centered on the #3 dacite porphyry. Epithermal Pb–Zn–Ag veins (quartz–galena–sphalerite) are associated with propylitic alteration in the medial and distal zones (JGEB 1996). Cu–Au ores, predominantly in wide veins (quartz–pyrite–chalcopyrite, commonly 0.5–1 cm wide, with some examples up to 15 cm), are associated with phyllic alteration in the proximal zone (Fig. 1d; JGEB 1996). Pb–Zn–Ag veins occur primarily at shallow levels, and Cu–Au veins have a large vertical extent, gradually

transitioning into small veins and disseminated ore at depth (JGEB 1996).

Previous chronological work on the Yinshan deposit

Li et al. (2007) reported a SHRIMP zircon U–Pb age of 183±3 Ma for the main dacite porphyry. Recent LA-ICPMS zircon U–Pb dating (Wang et al. 2012a; Liu et al. 2013) gives ages of 176±1 Ma for the principal hornblende rhyolite, and of 170–176 Ma for the early intrusives (dacite porphyry, quartz porphyry, and quartz diorite porphyry) at Yinshan. Wang et al. (2012a) also defined an age of 166±1 Ma for late andesite porphyry at the site. These radiometric ages demonstrate significant diachroneiety of intrusive events at Yinshan. Li et al. (2007) also obtained muscovite ^{40}Ar–^{39}Ar ages of ~175–178 Ma for the hydrothermally altered porphyry and interpreted this as the mineralization age for the deposit. Li et al. (2005) reported younger illite K–Ar ages of 122–136 Ma for the altered porphyries, which arguably date the post-emplacement exhumation and cooling of the system.

Results

Re–Os geochronology

Six molybdenite samples were analyzed in this study (Table 1 in Appendix II). They show variable Re contents (50.07–604.7 ppm) and low common Os contents (0.0889–3.378 ppm), yielding consistent individual calculated model ages between 165.1 and 170.3 Ma. Combined synthesis of all six analyses yields an isochron age of 170.3±2.5 Ma (Fig. 2).

(U–Th)/He thermochronology

Sample 10DX89 is a slightly K-altered granodiorite porphyry, collected from the Tongchang open pit of the Dexing mine (Table 2 in Appendix II). Four zircon grains from this sample yielded (U–Th)/He (ZHe) ages ranging from 110 to 120 Ma with a weighted mean of 114.4±4.8 Ma (Fig. 3a and Table 3 in Appendix II). Three apatite grains yielded (U–Th)/He (AHe) ages ranging from 7 to 9 Ma with a weighted average age of 8.0±1.6 Ma (Fig. 3b).

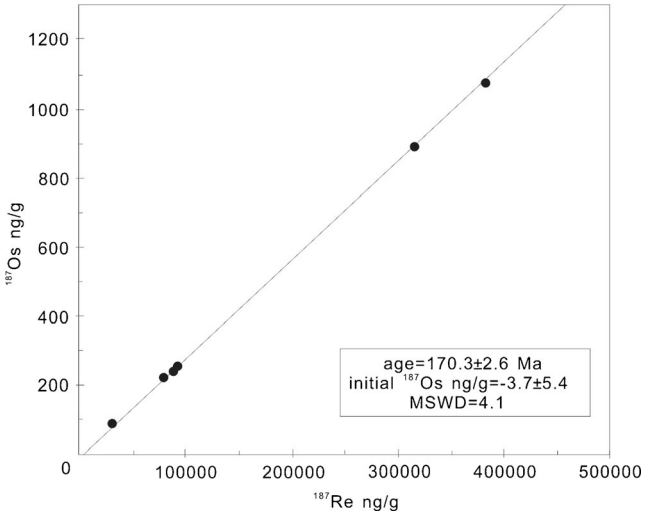

Fig. 2 Molybdenite Re-Os isochron for the Dexing deposit

Sample 10YS10 is a dacite porphyry sample with strong phyllic alteration, collected from the #3 porphyry of the Yinshan mine (Table 2 in Appendix II). Three zircon grains were dated, yielding ZHe ages ranging from 128 to 140 Ma with a weighted mean of 132.6±6.7 Ma (Fig. 3a). Three apatite grains yielded a consistent AHe age of 29.6±1.6 Ma (Fig. 3b).

Discussion

Magmatic to hydrothermal cooling

Cooling from magmatic through hydrothermal conditions in a porphyry deposit encompasses a history that begins with

Table 1 Molybdenite Re–Os isotopic results for the Dexing deposit

Sample name	Weight (g)	$w_{(Re)}$/μg.g^{-1}		$w_{(common\ Os)}$/ng.g^{-1}		$\omega_{(187Re)}$/μg.g^{-1}		$\omega(_{187Os})$/ng.g^{-1}		Model age (Ma)	
		Value	Uncertainty (2σ)	Value	Uncertainty (2σ)	Value	Uncertainty (2σ)	Value	Uncertainty (2σ)	Value	Uncertainty (2σ)
10DX99	0.0052	498.3	4	0.1015	0.1609	313.2	2.5	889.6	6.9	170.3	2.3
10DX160	0.00518	50.07	0.54	0.1188	0.3996	31.47	0.34	88.43	0.76	168.4	2.7
10DX100	0.00564	604.7	5.3	0.0889	0.3984	380.1	3.3	1076	9	169.7	2.4
10DX157	0.00532	143.1	1.1	0.1117	0.7512	89.94	0.7	250	2.5	166.6	2.5
10DX181	0.00524	137.1	1.2	0.1131	0.3803	86.17	0.73	237.3	2.2	165.1	2.5
10DX190	0.00528	121.8	1	3.378	0.376	76.56	0.62	214.7	2.1	168.1	2.5

Table 2 Sample location and petrologic descriptions

Sample No.	Locality	Elevation (above the sea level)	Petrology
10DX89	Tongchang open pit, Dexing deposit	80 m	Porphyritic texture; greenish; phenocrysts contains plagioclase, quartz, hornblende, biotite; matrix consists of the same mineral assemblage; feldspar phenocryst and matrix were sometimes replaced by secondary K-feldspar and biotite
10YS10	Jiuqu open pit of the Yinshan deposit	48 m	Porphyritic texture; gray in color; primary phenocrysts including feldspar, biotite and minor hornblende were strongly replaced by hydrothermal sericite

intrusion of porphyry stocks and effectively continues until the intrusion and country rocks have reached thermal equilibrium. Adopting 750 °C as the magmatic temperature (with the timing of crystallization provided by the zircon U–Pb closure temperature) and 200 °C for the ZHe closure temperature, the cooling rates of typical shallow level porphyry deposits may range from several hundred to several thousand °C per million years (°C/Ma; McInnes et al. 2005a; Harris et al. 2008; Li et al. 2012, 2014). Using these temperature points for the Dexing and Yinshan deposits, however, yields respective

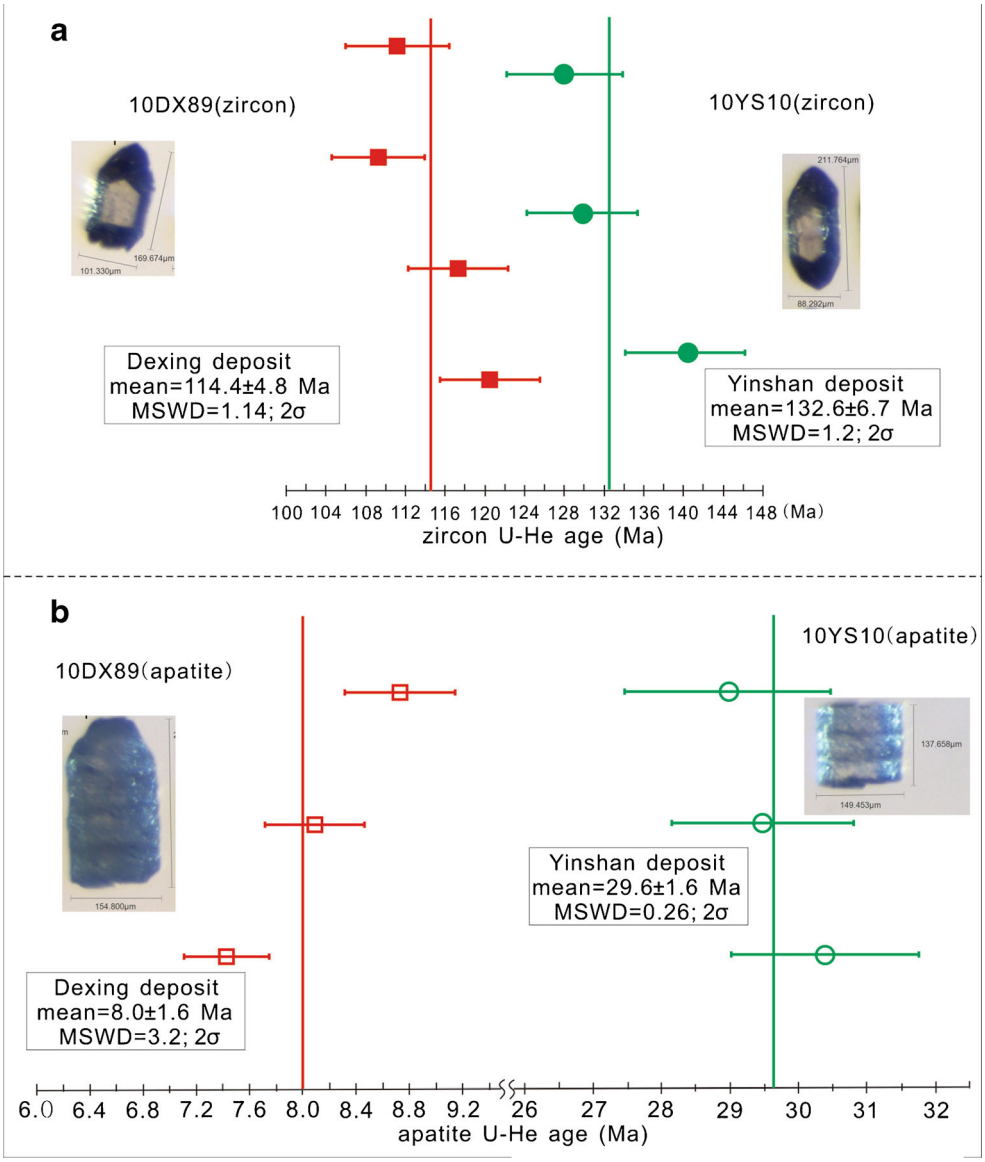

Fig. 3 Graphs of weighted average zircon (**a**) and apatite (**b**) U–He ages for the Dexing and Yinshan deposits

Table 3 (U–Th)/He thermochronology results

		^{232}Th (ng)	Th error (%)	^{238}U (ng)	U error (%)	U (ppm)	1 sigma	Th (ppm)	1 sigma	He (ncc)	He error (%)	TAU (%)	Th/U	Unc. age	±1σ	Ft	Corrected age (Ma)	±1σ
Apatite	10YS10-1	0.33	4.00	0.08	4.12	19.4	0.8	77.6	3.1	0.43	2.83	4.0	4.0	22.26	0.90	0.73	30.39	1.37
	10YS10-2	0.30	4.00	0.14	4.17	24.5	1.0	52.3	2.1	0.57	2.64	4.1	2.1	22.35	0.91	0.76	29.47	1.33
	10YS10-3	0.10	4.01	0.02	4.01	7.04	0.28	30.0	1.2	0.12	3.86	4.8	4.3	20.58	0.99	0.71	28.96	1.50
Zircon	10YS10-1	0.93	4.58	2.35	3.04	782	24	307	14	33.0	2.5	3.8	0.39	104.71	3.95	0.75	140.29	5.99
	10YS10-2	1.33	4.58	3.40	3.00	942	28	366	17	45.1	2.5	3.8	0.39	99.10	3.72	0.76	129.91	5.53
	10YS10-3	1.37	4.58	2.75	3.49	1358	47	671	31	34.4	2.6	4.1	0.49	91.37	3.74	0.71	128.14	5.84
Apatite	10DX89-1	0.86	4.00	0.39	4.30	34.1	1.5	74.6	3.0	0.43	2.84	4.2	2.2	5.96	0.25	0.80	7.42	0.32
	10DX89-2	0.33	4.00	0.13	4.04	19.6	0.8	50.7	2.0	0.15	2.96	4.2	2.6	6.07	0.25	0.75	8.09	0.37
	10DX89-3	0.50	4.00	0.21	4.26	22.4	1.0	53.4	2.1	0.28	3.00	4.3	2.4	6.92	0.30	0.79	8.73	0.41
Zircon	10DX89-1	1.60	4.58	2.50	3.05	768	23	487	22	31.8	2.5	3.7	0.64	90.46	3.34	0.75	120.50	5.06
	10DX89-2	1.96	4.58	2.93	3.08	759	23	504	23	37.3	2.5	3.7	0.66	89.63	3.32	0.76	117.34	4.94
	10DX89-3	1.44	4.58	1.83	3.02	697	21	544	25	20.9	2.6	3.7	0.78	78.99	2.92	0.72	109.31	4.60
	10DX89-4	1.33	4.58	1.71	3.02	1031	31	795	36	19.1	2.5	3.6	0.77	76.94	2.81	0.69	111.18	5.25

Note: U and Th ppm are approximate. They are calculated from microscopy grain measurements and assumed mineral densities (3.16 and 4.65 g/cc for apatite and zircon, respectively)

cooling rates of 10 °C/Ma and ~15 °C/Ma, which are 1 to 2 orders of magnitude lower than these typical figures.

This apparent discrepancy can be resolved in either of two ways—the original helium ages defining post-emplacement cooling could have been reset by later re-heating of the system, or the currently exposed porphyry systems may have developed deeper than typical for economic porphyry systems, at ambient conditions hotter than the ZHe closure temperature. The geological context of the Dexing system seems to favor the first of these alternatives—with evidence pointing to multiple episodes of significant post-emplacement heating of the porphyry body. Intrusion of a suite of quartz diorite dykes at ~154 Ma and K–Ar ages of K-feldspar (152–157 Ma) from quartz–K-feldspar veins support the introduction of significant heat at this time (Fig. 4a; Table 4 in Appendix II). For lower temperature constraints, however (ca. 200 °C for ZHe and 150 °C for Ar in illite—Hamilton et al. 1989), this event is overprinted at approximately 110 Ma, pointing to partial to complete loss of radiogenic He and Ar in the late Cretaceous. At Yinshan too, a small but distinctive volume of andesite porphyry formed after the main body at ~166 Ma. As at Dexing, these intrusions may have introduced significant heat, overprinting the primary cooling ages of the system (Fig. 4b; Table 4 in Appendix II). The thermal bounds of such reheating are highly under-constrained, but we suggest the temperatures experienced may have been sufficient to reset ZHe ages for the porphyry.

The alternative of emplacement at ambient temperatures near or above the blocking temperature for helium in zircon (as at the Ciemas Cu deposit, Indonesia; McInnes et al. 2005a, 2005b) is considered unlikely for these systems—particularly Yinshan. Although high homogenization pressures (corresponding to minimum paleo-depths of ~6 km) were obtained from fluid inclusions within early A type veins for Dexing (Pan et al. 2009; our unpublished data), this still corresponds to background conditions of only ca. 150 °C (assuming a geothermal gradient of 25 °C/km)—high enough to perhaps slow post-emplacement cooling somewhat, but still nowhere near the levels required to maintain open system ZHe behavior for the 40 to 50 million years indicated. Such a mechanism is even less tenable for the Yinshan system. Geological and fluid inclusion evidence point to the Yinshan deposit as the shallow manifestation of a deeper porphyry system, with formation of the exposed elements of mineralization limited to <4 km depth (Wang et al. 2013)—far too shallow to account for delayed ZHe closure.

Exhumation

Late stage cooling that cannot be associated with intrusive emplacement, hydrothermal veining, or other mechanism of significant heat flux is most likely to represent progressive solid state cooling during unroofing and exhumation (McInnes et al. 2005a). AHe dating provides the clearest guide to the timing of such late exhumation, with its closure at low nominal temperatures of around 70 °C (Farley 2000) affording the greatest possible distinction from typical hydrothermal and other near-surface activity (McInnes et al. 1999, 2005a; Arehart et al. 2003; Chakurian et al. 2003; Harris et al. 2008; Li et al. 2012; Zeng et al. 2013).

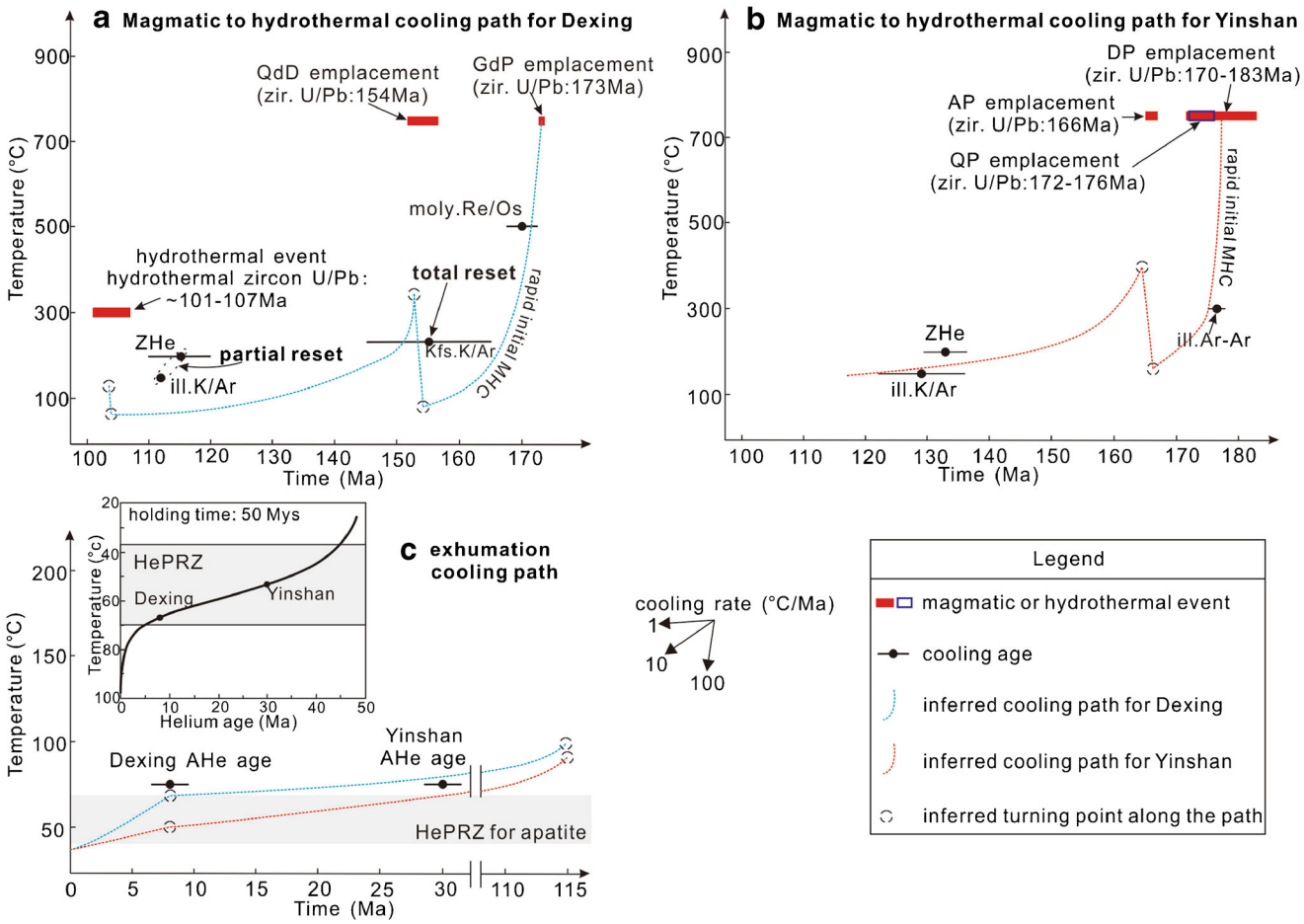

Fig. 4 Graphs of possible magmatic to hydrothermal cooling paths for the Dexing (**a**) and Yinshan (**b**) deposits; and possible exhumation cooling path for both of Dexing and Yinshan (**c**). *Inset* is adapted from the Fig. 2 of Wolf et al. (1998) illustrating an apatite helium partial retention zone (HePRZ) by isothermal holding for 50 Ma. Note that the cooling paths are constructed in a qualitative sense, and thus, cannot be used quantitatively to determine temperatures at a given time. Age data are from Table 4. *GdP* granodiorite porphyry, *QdD* quartz diorite porphyry dyke, *QP* quartz porphyry, *DP* dacite porphyry, *AP* andesite porphyry, *zir.* zircon, *moly.* molybdenite, *Kfs.* K-feldspar, *ill.* illite, *bio.* biotite, *MHC* magmatic to hydrothermal cooling, *ZHe* zircon helium age, *AHe* apatite helium age

Perhaps the most significant distinction between the Yinshan and Dexing geo-thermochronometry data sets is the ~20-million-year difference between the AHe ages of the two deposits. Assuming that the Dexing region has an average continental geothermal gradient of around 25 °C/km and a mean annual surface temperature of 20 °C, these apatite (U–Th)/He ages define the time when each deposit was eroded to within 2 km of the paleo-surface (McInnes et al. 1999, 2005a, b). The older AHe age of the Yinshan deposit is consistent with some combination of earlier, slower, and/or shallower exhumation relative to the Dexing deposit. The relative contributions of these three variables are impossible to directly assess, but the comparative geology of the two deposits favors the third factor—differential exhumation—as a significant contribution.

Dexing contains typical porphyry mineralization consistent with emplacement at depths of 2–5 km, whereas the veining and alteration present at Yinshan argues for a mineral endowment developed at shallower crustal levels. The shallower Yinshan deposit may have sat within the partial retention zone for helium in apatite (Fig. 4c inset; the range of crustal depths corresponding to temperatures between ca. 40 °C and 70 °C, under which conditions diffusion of helium is just fast enough that a portion of that daughter product created by radioactive decay of U and Th is retained on geological timescales) for an extended period leading up to final exhumation. On the contrast, the deeper Dexing deposit may have remained below this depth and experiencing complete loss of its radiogenic helium. Therefore, the variable depth alone could account for the difference in AHe age (Fig. 4c). Subsequent exhumation and cooling of the two deposits at or around 8 Ma would be recorded relatively faithfully as an event in the Dexing Deposit—the AHe age of which was held at zero prior to this final phase of cooling—but the helium built up within apatite at Yinshan during its residence in the PRZ would result in older apparent ages, despite experiencing final uplift and cooling at the same time.

Table 4 Summary of geochronological and thermochronological data from the Dexing and Yinshan deposits

Chronometer	*Tc* used (°C)		Dexing			Yinshan		
	Value	Reference	Host rock	Age (Ma)	Reference	Host rock	Age (Ma)	Reference
Zircon U–Pb	750	Reiners (2005)	Fresh granodioritic porphyry	172.5±0.5	Liu et al.(2012)	Porphyry stocks with phyllic alteration	170–183	Li et al. (2007); Wang et al. (2012a); Liu et al. (2013)
			Quartz dioritic dyke	153.5±2.4	Zhou et al. (2012a)	Andesitic porphyry	166+/−1	Wang et al. (2012a)
			Pyrite–chalcopyrite–quartz vein	101–107	Zhou et al. (2012b)			
Molybdenite Re–Os	500	Suzuki et al. (1996)	Molybdenite–pyrite–quartz vein	170.3±2.6	This paper			
Illite Ar–Ar	300					Porphyry stocks with phyllic alteration	175–178	Li et al. (2007)
K-feldspar K–Ar	230		Quartz–K-feldspar vein	154.5±10	Zhu et al.(1983)			
ZHe	200	Reiners (2005)	Granodioritic porphyry with slight potassic alteration	114.4±4.8	This paper	Dacitic porphyry with phyllic alteration	132.6±6.7	This paper
Illite K–Ar	150	Hamilton et al. (1989)	Granodioritic porphyry with phyllic alteration	112	Zhu et al.(1983)	Dacitic porphyry with phyllic alteration	122–125	Li et al. (2005)
AHe	75	Reiners (2005)	Granodioritic porphyry with slight potassic alteration	8.0±1.6	This paper	Dacitic porphyry with phyllic alteration	29.6±1.6	This paper

Exploration implications

Diamond drilling has revealed that the wide Cu–Au bearing sulfide veins at Yinshan gradually transition into smaller veins and disseminated ore at depth (JGEB Jiangxi Geological Exploration Bureau 1996). Recent geochemical, geochronological, and isotopic studies have demonstrated that the dacite porphyries at Yinshan and granodiorite porphyries at Dexing were emplaced contemporaneously, and probably, originated from a similar source (Liu et al. 2012, 2013; Wang et al. 2012a). These characteristics indicate that the ore-forming magmas at Yinshan have a similar potential for forming porphyry-style copper mineralization to that of Dexing. The differential exhumation between the two ore deposits in the Late Cenozoic indicated by our (U–Th)/He data led to the exposure of the Dexing porphyry ore bodies, while equivalent mineralization at Yinshan would remain concealed at depth, supporting the hypothesis that a porphyry Cu–Au deposit may exist below the current Yinshan mine.

In addition, our study indicates that the Middle Jurassic porphyry copper systems of the Dexing region may have been preserved under relatively stable crustal conditions for a protracted period. Such favorable preservation conditions may arise from the post-Jurassic tectonically quiescent non-arc or intraplate tectonic setting of the Dexing region (Wang et al. 2006; Liu et al. 2012). Such intraplate regions could be prospective for porphyry Cu systems like Dexing and Yinshan, if post-subduction remelting of the pre-fertilized lithosphere has occurred (Richards 2011).

Conclusions

The cooling ages of the Dexing copper deposit post-date primary crystallization of the major associated porphyry system. In light of the relatively deep primary intrusion of this body, recorded zircon (U–Th)/He ages may reflect post emplacement exhumation, but independent evidence for later intrusive activity and late mineralization at ~154 and ~105 Ma indicates these ZHe ages most likely reflect thermal re-setting of the system. The recorded cooling ages of the Yinshan polymetallic deposit may similarly reflect disturbance and resetting of early ingrowth of helium by an intrusive event at ~166 Ma and/or by burial heating in the Early Cretaceous.

Subsequent to these Jurassic–Cretaceous thermal excursions, both the Dexing and Yinshan deposits appear to have experienced relative stasis within or immediately below the apatite helium partial retention zone (ca. 40–70 °C). Similarities in timing and mineralogy between the two deposits suggest that their differences in style and tenor may arise largely from differential exhumation—with the Yinshan

deposit a less-exhumed equivalent of the Dexing deposit. It follows that porphyry-style mineralization similar to that at Dexing may exist at depth under the current Yinshan mine.

Acknowledgements We wish to thank Allen Thomas and Cameron Scadding (TSW™ Analytical) for assistance with ICPMS analysis and Celia Mayers and Brad McDonald for grain selection for thermochronology. Kind help from Wenjun Qu and Chao Li during molybdenite Re–Os analysis is gratefully acknowledged. Dr. Junxing Zhao provided useful discussion and comments. Dr. Diego Villagomez, an anonymous reviewer, and the Associate Editor Thomas Bissig are thanked for their constructive and valuable comments which greatly contributed to improvement of the manuscript. This research was financially supported by the Student Research Grant (Hugh E. McKinstry Fund of 2012) of the Society of Economic Geologists granted to X. Liu, and the Intellectual Innovation Project, Chinese Academy of Sciences (KZCX1-YW-15-3).

Appendix

Methodology

Re–Os geochronology

Molybdenite Re–Os isotopic analysis on samples from the Dexing deposit was conducted at the National Research Center for Geoanalysis (NRCG), Chinese Academy of Geological Sciences. Analytical conditions and analytical procedures are the same as those described by Yang et al. (2005). Re and Os concentrations were determined by isotope dilution. The ^{185}Re and ^{190}Os spikes were obtained from Oak Ridge National Laboratory, USA, and calibrated at NRCG. Molybdenite was separated from six molybdenite–pyrite–quartz veins with more than 1.0 g molybdenite selected from each vein. Accurately weighed 0.2 g aliquots were selected from the <200 mesh material, loaded into Carius tubes, together with ^{185}Re and ^{190}Os spikes, and digested by reverse aqua regia. Os was separated as OsO_4 by distillation at 105–110 °C and trapped by Milli-Q water. The residue solutions were diluted with distilled water and dried. The solids were then dissolved in a 5 M NaOH solution, from which Re was extracted by acetone.

Re and Os isotopic compositions were determined using an Inductively Coupled Plasma Mass-spectrometer (ICP-MS, PQ Excell). The intensity of the ^{190}Os signal was monitored to correct for trace Os in Re, and ^{185}Re was used to monitor trace Re in Os. 5 % ammonia; and H_2O_2 were repeatedly used to wash the Teflon injection tube in order to avoid cross-contamination. The total procedural blanks were 20 to 30 pg for Re and 1 pg for Os, based on blanks analyzed with the samples. The background ^{187}Os/^{188}Os was 0.25 based on routine repeated blank measurement. The accuracy of the analysis was controlled by laboratory reference sample JDC (molybdenite from the Jinduicheng ore deposit, Du et al. 2004).

(U–Th)/He thermochronology

Zircon and apatite (U–Th)/He thermochronology was performed in the John de Laeter Center for Isotope Research, Curtin University. Euhedral zircon and apatite grains were selected under a long working distance binocular microscope. Individual grains were visually interrogated in plain and cross-polarized light in order to detect and remove material containing U- and/or Th-rich mineral or fluid inclusions that may contribute excess helium. Measurements were recorded for each grain for calculation of the alpha correction (Farley et al. 1996), and images of selected grains were recorded digitally (Fig. 4). Grains with a diameter greater than 70 μm were preferred where possible in order to ensure helium gas values were optimal for measurement and to minimize the alpha ejection correction. Characterized grains were loaded into niobium (zircon) or platinum (apatite) microvials. Helium was thermally extracted from each individual encapsulated crystal using a 1,064-nm Nd-YAG laser. ^{4}He abundances were determined by isotope dilution method using a pure ^{3}He spike, calibrated daily against an independent ^{4}He standard tank. Uncertainty in the sample ^{4}He measurement was <1 %.

For zircon, the U and Th content were determined using isotope dilution ICP-MS. Samples were removed from the laser chamber and transferred to Parr pressure dissolution vessels where they were spiked with ^{235}U and ^{230}Th (25 μl of a solution containing 15 ppb ^{235}U and 15 ppb ^{230}Th) and digested at 240 °C for 40 h in 350 μl of HF. Standard solutions were spiked and treated similarly, as were a series of unspiked reagent blanks. After dissolution, samples were removed from the pressure vessels and allowed to dry for 2 days. Three hundred microliters of HCl was added to each vial, which was then subjected to a second bombing for 24 h at 200 °C to ensure dissolution of fluoride salts. Final solutions were diluted to 10 % acidity for analysis on an Agilent 7500CS mass spectrometer (TSW™ Analytical). For single crystals digested in small volumes (0.3–0.5 ml), U and Th isotope ratios were measured to a precision of <2 % (Evans et al. 2005). Repeated measurement of internal age standards by zircon (U–Th)/He methods at Curtin has an estimated precision of <6 %.

For degassed apatite, the U and Th content were determined by isotope dilution using ^{235}U and ^{230}Th spikes. Twenty-five microliters of a 50 % (by volume; approximately 7 M) HNO_3 solution containing approximately 15 ppb ^{235}U and 5 ppb ^{230}Th was added to each sample. The apatite was digested in the spiked acid for at least 12 hours to allow the spike and sample isotopes to equilibrate. Standard solutions containing 27.6 ppb U and 28.4 ppb Th, were spiked and treated identically to samples, as were a series of unspiked reagent blanks. Two hundred fifty microliters of Milli-Q water was added prior to analysis on an

Agilent 7500CS mass spectrometer. U and Th isotope ratios were measured to a precision of <2 %. Overall apatite (U–Th)/He thermochronology analysis at Curtin has a precision of 2.5 %, based on multiple age determinations (n=26) of Durango standard which produce an average age of 31.1±1.0 (2σ)Ma.

References

Arehart GB, Chakurian AM, Tretbar DR, Christensen JN, McInnes BA, Donelick AR (2003) Evaluation of radioisotope dating of Carlin-type deposits in the Great Basin, Western North America, and implications for deposit genesis. Econ Geol 98:235–248

Chakurian AM, Arehart GB, Donelick RA, Zhang X, Reiners PW (2003) Timing constraints of gold mineralization along the Carlin Trend utilizing apatite fission-track, $^{40}Ar/^{39}Ar$, and apatite (U-Th)/He methods. Econ Geol 98:1159–1171

Cherniak DJ, Watson EB (2000) Pb diffusion in zircon. Chem Geol 172: 5–24

Du AD, Wu SQ, Sun DZ, Wang SX, Qu WJ, Markey R, Stein H, Morgan J, Malinovskiy D (2004) Preparation and certification of Re-Os dating reference materials: molybdenite HLP and JDC. Geostand Geoanal Res 28:41–52

Evans NJ, Wilson NSF, Cline JS, McInnes BIA, Byrne J (2005) Fluorite (U-Th)/He thermochronology: constraints on the low temperature history of Yucca Mountain, Nevada. Appl Geochem 20:1099–1105

Farley KA (2000) Helium diffusion from apatite: general behavior as illustrated by Durango fluorapatite. J Geophys Res 105:2903–2914

Farley KA, Stöckli DF (2002) (U-Th)/He dating of phosphates: apatite, monazite, and xenotime. Rev Mineral Geochem 48:559–577

Farley KA, Wolf RA, Silver LT (1996) The effects of long alpha-stopping distances on (U-Th)/He ages. Geochim Cosmochim Ac 60:4223–4229

Hamilton PJ, Kelley S, Fallick AE (1989) K-Ar dating of illite in hydrocarbon reservoirs. Clay Miner 24:215–231

Harris A, Dunlap WJ, Reiners PW, Allen CM, Cooke DR, White NC, Campbell IH, Golding SD (2008) Multimillion year thermal history of a porphyry copper deposit: application of U–Pb, $^{40}Ar/^{39}Ar$ and (U–Th)/He chronometers, Bajo de la Alumbrera copper–gold deposit, Argentina. Miner Deposita 43:295–314

Hou Z, Pan X, Li QY, Yang ZM, Song YC (2013) The giant Dexing porphyry Cu-Mo-Au deposit in east China: product of melting of juvenile lower crust in an intracontinental setting. Miner Deposita 1–27

Hua RM, Li XF, Lu JJ, Chen PR, Qiu DT, Wang G (2000) Study on the tectonic setting and ore-forming fluids of Dexing large ore-concentrating area, northeast Jiangxi province. Adv Earth Sci 15: 525–533, in Chinese with English abstract

Huang CK, Bai Y, Zhu YS, Wang HZ, Shang XZ (2001) Copper deposits of China. Geological Publishing House, Beijing, pp 57–72 (in Chinese with English abstract)

JGB (Jiangxi Geological Bureau) (1980) Report on regional geology of the People's Republic of China (Leping area of Jiangxi Province). Geological Publishing House, Beijing, pp 104–123 (in Chinese with English abstract)

JGEB (Jiangxi Geological Exploration Bureau) (1996) Yinshan Cu-Pb-Zn-Au-Ag deposit in Jiangxi Province. Geological Publishing House, Beijing, p 380 (in Chinese with English abstract)

Kesler SE, Wilkinson BH (2006) The role of exhumation in the temporal distribution of ore deposits. Econ Geol 101:919–922

Li XF, Wang C, Mao JW, Hua RM, Liu YN, Xu QH (2005) Kübler index and K-Ar ages of illite in the Yinshan polymetallic deposit, Jiangxi province, south China: Analyses and implications. Resour Geol 55: 397–404

Li XF, Watanabe Y, Mao JW, Liu SX, Yi XK (2007) Sensitive High-Resolution Ion Microprobe U-Pb zircon and ^{40}Ar-^{39}Ar muscovite ages of the Yinshan deposit in the northeast Jiangxi province, South China. Resour Geol 57:325–337

Li XH, Li WX, Li ZX, Lo CH, Wang J, Ye MF, Yang YH (2009) Amalgamation between the Yangtze and Cathaysia Blocks in South China: constraints from SHRIMP U-Pb zircon ages, geochemistry and Nd-Hf isotopes of the Shuangxiwu volcanic rocks. Precambrian Res 174:117–128

Li JX, Qin KZ, Li GM, Cao MJ, Xiao B, Chen L, Zhao JX, Evans NJ, McInnes BIA (2012) Petrogenesis and thermal history of the Yulong porphyry copper deposit, Eastern Tibet: insights from U-Pb and U-Th/He dating, and zircon Hf isotope and trace element analysis. Mineral Petrol 105:201–221

Li GM, Cao MJ, Qin KZ, Evans NJ, McInnes BIA, Liu YS (2014) Thermal-tectonic history of the Baogutu porphyry Cu deposit, West Junggar as constrained from zircon U–Pb, biotite Ar/Ar and zircon/apatite (U–Th)/He dating. J Asian Earth Sci 79:741–758

Liu X, Fan HR, Santosh M, Hu FF, Yang KF, Li QL, Yang YH, Liu YS (2012) Remelting of Neoproterozoic relict volcanic arcs in the Middle Jurassic: implication for the formation of the Dexing porphyry copper deposit, Southeastern China. Lithos 150:85–100

Liu X, Fan HR, Santosh M, Hu FF, Yang KF, Wen BJ, Yang YH, Liu YS (2013) Origin of the Yinshan epithermal-porphyry Cu-Au-Pb-Zn-Ag deposit, SE China: insights from geochemistry, Sr-Nd and zircon U-Pb-Hf-O isotopes. Int Geol Rev 55:1835–1864

McInnes BIA, Farley KA, Sillitoe RH, Kohn BP (1999) Application of apatite (U-Th)/He thermochronometry to the determination of the sense and amount of vertical fault displacement at the Chuquicamata porphyry copper deposit, Chile. Econ Geol 94: 937–947

McInnes BIA, Evans NJ, Fu FQ, Garwin S (2005a) Application of thermochronology to hydrothermal ore deposits. Rev Mineral Geochem 58:467–498

McInnes BIA, Evans NJ, Fu FQ, Garwin S, Belousova E, Griffin WL, Bertens A, Sukarna D, Permanadewi S, Andrew RL, Deckart K (2005b) Thermal history analysis of select Chilean, Indonesian and Iranian porphyry Cu-Mo-Au deposits. In: Porter TM (ed) Super porphyry copper and gold deposits—a global perspective. PGC Publishing, Adelaide, pp 27–42

Pan XF, Song YC, Wang SX, Li ZQ, Yang ZM, Hou ZQ (2009) Evolution of hydrothermal fluid of Dexing Tongchang copper-gold porphyry deposit. Acta Geol Sin 12:1929–1950 (in Chinese with English abstract)

Reiners PW (2005) Zircon (U-Th)/He thermochronometry. Rev Miner Geochem 58:151–179

Reiners PW, Farley KA (1999) He diffusion and (U-Th)/He thermochronometry of titanite. Geochim Cosmochim Ac 63:3845–3859

Richards JP (2011) Magmatic to hydrothermal metal fluxes in convergent and collided margins. Ore Geol Rev 40:1–26

Seedorff E, Dilles JH, Proffett JM, Jr., Einaudi MR, Zurcher L,Stavast WJA, Johnson DA, Barton MD (2005) Porphyry copper deposits: characteristics and origin of hypogene features. Econ Geol Economic Geology 100th Anniversary Volume: 251–298

Selby D, Creaser RA (2001) Re-Os geochronology and systematics in molybdenite from the Endako porphyry molybdenum deposit, British Columbia, Canada. Econ Geol 96:197–204

Suzuki K, Shimizu H, Masuada A (1996) Re-Os dating of molybdenites from ore deposits in Japan: Implication for the closure temperature of the Re-Os system for molybdenite and the cooling history of molybdenum in ore deposits. Geochim Cosmochim Ac 60:3151–3159

Wang Q, Xu JF, Jian P, Bao ZW, Zhao ZH, Li CF, Xiong XL, Ma JL (2006) Petrogenesis of adakitic porphyries in an extensional tectonic setting, Dexing, South China: implications for the genesis of porphyry copper mineralization. J Petro 47:119–144

Wang XL, Zhao GC, Zhou JC, Liu YS, Hu J (2008) Geochronology and Hf isotopes of zircon from volcanic rocks of the Shuangqiaoshan Group. South China: implications for the Neoproterozoic tectonic evolution of the eastern Jiangnan orogen. Gondwana Res 14:355–367

Wang GG, Ni P, Zhao KD, Wang XL, Liu JQ, Jiang SY, Chen H (2012a) Petrogenesis of the Middle Jurassic Yinshan volcanic-intrusive complex, SE China: implications for tectonic evolution and Cu-Au mineralization. Lithos 150:135–154

Wang W, Zhou MF, Yan DP, Li JW (2012b) Depositional age, provenance, and tectonic setting of the Neoproterozoic Sibao Group, southeastern Yangtze Block, South China. Precambrian Res 192–195:107–124

Wang GG, Ni P, Wang RC, Zhao KD, Chen H, Ding JY, Zhao C, Cai YT (2013) Geological, fluid inclusion and isotopic studies of the Yinshan Cu-Au-Pb-Zn-Ag deposit, South China: Implications for ore genesis and exploration. J Asian Earth Sci 74:343–360

Wolf RA, Farley KA, Silver LT (1996) Helium diffusion and low-temperature thermochronometry of apatite. Geochim Cosmochim Ac 60:4231–4240

Wolf RA, Farley KA, Kass DM (1998) A sensitivity analysis of the apatite (U-Th)/He thermochronometer. Chem Geo 148:105–114

Yang G, Du AD, Lu JR, Qu WJ, Chen JF (2005) Re-Os (ICP-MS) dating of the massive sulfide ores from the Jinchuan Ni-Cu-PGE deposit. Sci China Ser D 48:1672–1677

Zeng Q, Evans NJ, McInnes BIA, Batt GE, McCuaig CT, Bagas L, Tohver E (2013) Geological and thermochronological studies of the Dashui gold deposit, West Qinling Orogen, Central China. Miner Deposita 48:397–412

Zhou Q, Jiang YH, Zhao P, Liao SY, Jin GD (2011) Origin of the Dexing Cu-bearing porphyries, SE China: elemental and Sr-Nd-Pb-Hf isotopic constraints. Int Geol Rev 54:572–592

Zhou Q, Jiang YH, Liao SY, Zhao P, Jin GD, Jia RY, Liu Z, Xu XS (2012a) SHRIMP zircon U-Pb dating and Hf isotope studies of the diorite porphyrite from the Dexing copper deposit. Acta Geol Sin 86:1726–1734 (in Chinese with English abstract)

Zhou Q, Jiang YH, Zhao P, Liao SY, Jin GD, Liu Z, Jia RY (2012b) SHRIMP U-Pb dating on hydrothermal zircons: evidence for an early Cretaceous epithermal event in the middle Jurassic Dexing porphyry copper deposit, southeast China. Econ Geol 107:1507–1514

Zhu X, Hang CK, Rui ZY, Zhou YH, Zhu XJ, Hu CS, Mei ZK (1983) The geology of Dexing porphyry copper ore field. Geological Publishing House, Beijing, p 336, in Chinese with English abstract